Peridynamic Modeling of Large Deformation and Ductile Fracture

BROWN School of Engineering

Masoud Behzadinasab*, John T. Foster**, Yuri Bazilevs*

*School of Engineering, Brown University, Providence, RI

**Hildebrand Department of Petroleum & Geosystems Engineering, The University of Texas at Austin, Austin, TX

✉ masoud_behzadinasab@brown.edu

Abstract

• An unbiased investigation into the capabilities of peridynamics in simulating ductile fracture is undertaken.

• Some shortcomings associated with the Lagrangian, finite deformation peridynamic model are identified.

• A novel bond-associated, semi-Lagrangian, constitutive correspondence PD framework is proposed.

Peridynamic Theory

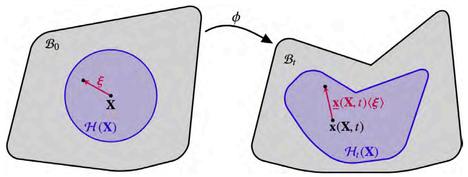

Figure 1. A peridynamic body mapped by a deformation state

- A *nonlocal* recast of the mechanics of solid deformations.
- Most previous PD models are Lagrangian formulations.

Classical (Lagrangian) equation of motion:

$$\rho_0\ddot{\mathbf{u}}(\mathbf{X},t) = \nabla\cdot\mathbf{P}(\mathbf{X},t) + \rho_0\mathbf{b}(\mathbf{X},t).$$

State-based peridynamic equation of motion:

$$\rho_0\ddot{\mathbf{u}}(\mathbf{X},t) = \int_{\mathcal{H}(\mathbf{X})} [\underline{\mathbf{T}}(\mathbf{X},t)\langle\boldsymbol{\xi}\rangle - \underline{\mathbf{T}}(\mathbf{X}+\boldsymbol{\xi},t)\langle-\boldsymbol{\xi}\rangle]\,\mathrm{d}\boldsymbol{\xi} + \rho_0\mathbf{b}(\mathbf{X},t),$$

- Material failure is typically achieved through bond breakage.
- Peridynamics has been mostly used in studying brittle fracture.

Sandia Fracture Challenge 2017

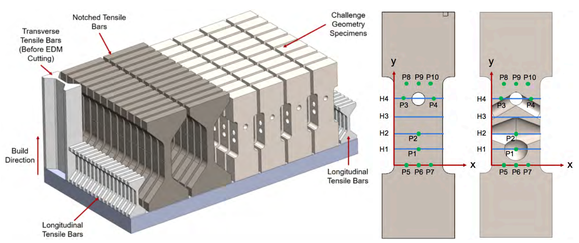

Figure 2. Layout of specimens in SFC3

- The third Sandia Fracture Challenge (SFC3) involved prediction of the mechanical behavior of an additively manufactured metal, given a set of common engineering calibration test data.
- We used the most recent peridynamic finite deformation and ductile fracture models to participate in the challenge.
- While our modeling approach led to acceptable predictions, including the correct crack path, it underpredicted the load-carrying capacity of the structure and simulated an early fracture.
- Main sources of error were identified as (1) material instabilities associated with the finite deformation peridynamic correpondence model and (2) unreliability of a Lagrangian peridynamic framework in solving problems involving large deformations.

Semi-Lagrangian PD

Everything is written in the current, deformed configuration.

$$\rho\frac{\mathrm{D}\dot{\mathbf{x}}}{\mathrm{D}t} = \mathbf{F} + \rho\mathbf{b}. \tag{1}$$

Let define a state-based internal state of a material point, i.e.,

$$\mathbf{F}(\mathbf{x}) = \int_{\mathcal{H}(\mathbf{x})} [\underline{\mathbf{t}}(\mathbf{x})\langle\boldsymbol{\eta}\rangle - \underline{\mathbf{t}}(\mathbf{x}+\boldsymbol{\eta})\langle-\boldsymbol{\eta}\rangle]\,\mathrm{d}\boldsymbol{\eta}, \tag{2}$$

$$\mathcal{H}(\mathbf{x}) = \{\mathbf{x}+\boldsymbol{\eta} \mid \mathbf{x}+\boldsymbol{\eta}\in\mathcal{B},\, 0<|\boldsymbol{\eta}|\le\delta\}.$$

Energy balance:

$$\frac{\mathrm{d}}{\mathrm{d}t}\int_{\mathcal{P}}\rho\dot{\mathbf{x}}\cdot\dot{\mathbf{x}}\,\mathrm{d}\mathbf{x} = \int_{\mathcal{P}}\mathbf{F}\cdot\dot{\mathbf{x}}\,\mathrm{d}\mathbf{x} + \int_{\mathcal{P}}\rho\mathbf{b}\cdot\dot{\mathbf{x}}\,\mathrm{d}\mathbf{x}. \tag{3}$$

Using (2) and (3) and rearranging, then comparing with the first law of thermodynamics, and localizng:

$$\dot{\mathrm{u}}(\mathbf{x}) = \int_{\mathcal{H}(\mathbf{x})}\underline{\mathbf{t}}(\mathbf{x})\langle\boldsymbol{\eta}\rangle\cdot\dot{\boldsymbol{\eta}}\,\mathrm{d}\boldsymbol{\eta}, \tag{4}$$

where u is called the *strain energy density*.

Correspondence Materials

A bond-associated velocity gradient tensor:

$$\underline{\mathbf{L}}(\mathbf{x})\langle\boldsymbol{\eta}\rangle = \frac{\bar{\mathbf{L}}(\mathbf{x})+\bar{\mathbf{L}}(\mathbf{x}+\boldsymbol{\eta})}{2} + \left(\dot{\boldsymbol{\eta}} - \frac{\bar{\mathbf{L}}(\mathbf{x})+\bar{\mathbf{L}}(\mathbf{x}+\boldsymbol{\eta})}{2}\cdot\boldsymbol{\eta}\right)\otimes\frac{\boldsymbol{\eta}}{|\boldsymbol{\eta}|^2}, \tag{5}$$

in which $\underline{\mathbf{L}}(\mathbf{x})\langle\boldsymbol{\eta}\rangle$ is the velocity gradient associated with the bond $\boldsymbol{\eta}$. $\bar{\mathbf{L}}(\mathbf{x})$ is the velocity gradient at $\mathbf{x}$, which is determined through an integration of the collective deformation of the neighborhood

$$\bar{\mathbf{L}}(\mathbf{x}) = \left(\int_{\mathcal{H}(\mathbf{x})}\underline{\omega}\langle\boldsymbol{\eta}\rangle\,\dot{\boldsymbol{\eta}}\otimes\boldsymbol{\eta}\,\mathrm{d}\boldsymbol{\eta}\right)\mathbf{M}^{-1}(\mathbf{x}), \tag{6}$$

$$\mathbf{M}(\mathbf{x}) = \int_{\mathcal{H}(\mathbf{x})}\underline{\omega}\langle\boldsymbol{\eta}\rangle\,\boldsymbol{\eta}\otimes\boldsymbol{\eta}\,\mathrm{d}\boldsymbol{\eta}, \tag{7}$$

where $\underline{\omega}$ is a weight function. According to the classical theory,

$$\underline{\dot{\mathrm{u}}}\langle\boldsymbol{\eta}\rangle = \dot{\psi}(\underline{\mathbf{L}}\langle\boldsymbol{\eta}\rangle) = \underline{\boldsymbol{\sigma}}\langle\boldsymbol{\eta}\rangle : \underline{\mathbf{L}}\langle\boldsymbol{\eta}\rangle, \tag{8}$$

where $\underline{\boldsymbol{\sigma}}$ is the bond Cauchy stress. Using (4) to (8), $\underline{\mathbf{t}}$ is obtained.

Bond-Associated Damage Correspondence Modeling

$$\underline{\omega}\langle\boldsymbol{\eta}\rangle = \omega_\eta(|\boldsymbol{\eta}|)\,\omega_D(\underline{D}\langle\boldsymbol{\eta}\rangle),$$

where $\omega_\eta(|\boldsymbol{\eta}|)$ is the conventional, spherical influence function for undamaged material. ω_D is required to be a non-increasing function of the bond-level damage $\underline{D}$, which is a function of the bond-level internal properties (e.g. plastic strain) and is determined using classical damage models.

A Revisit to SFC3

- The same discrete systems and calibration data as in the initial approach are used. Also, an isotropic, homogeneous material, with no dependency on rate of deformation or temperature, is considered.
- To maintain material objectivity, the numerical algorithm of Flanagan and Taylor (1987) is utilized to integrate an isotropic hardening power-law model in rate form using a co-rotational stress rate.
- A modified Brozzo's damage model (1972) is used to calculate damage by considering the plastic strain and hydrostatic stress.

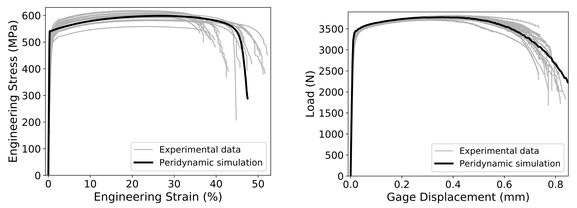

Figure 3. An inverse method is used to calibrate the model. Gray and black indicate experiments and simulations, respectively.

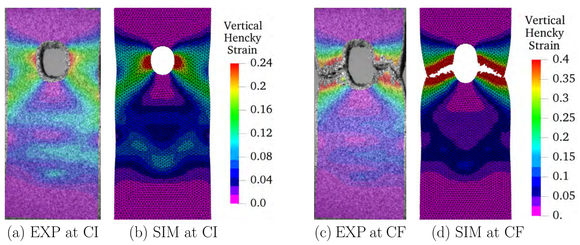

Figure 4. Vertical Hencky strains compared between the experimental DIC measurements (EXP) and peridynamic simulations (SIM) at crack initiation (a–b) and complete failure (c–d).

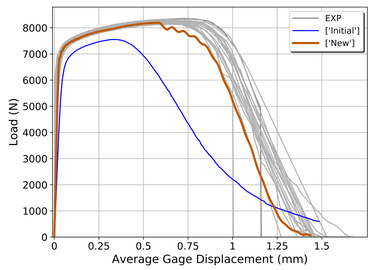

Figure 5. Macroscopic behavior of the challenge specimen compared between the initial and new simulations, and the experimental.

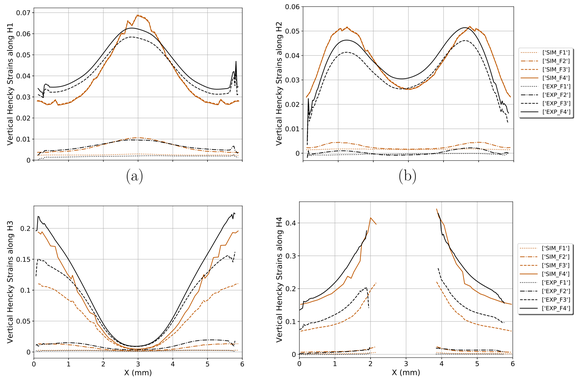

Figure 6. Vertical logarithmic strains along 4 lines H1 (a), H2 (b), H3 (c), and H4 (d) at four instances of loading F1, F2, F3, and F4.

Acknowledgements

This research receives funding through an AFOSR MURI Project and a UT Austin Graduate School Continuing Fellowship.

References

1. Behzadinasab M, Foster JT. *Int. J. Fract.*, 218(1):97–109 (2019)
2. Behzadinasab M, Foster JT. *Int. J. Solids. Struct.*, 182:64–76 (2020)
3. Behzadinasab M, Foster JT. *J. Mech. Phys. Solids*, 103862 (2020)
4. Behzadinasab M, Foster JT. *Int. J. Fract.* Submitted
5. Brozzo P, Deluca B, Rendina R. *Proc. 7th biennal Conf. IDDR*, (1972)
6. Flanagan DP, Taylor LM. *Comput. Methods Appl. Mech. Eng.*, 62(3):305–320 (1987)
7. Foster JT, Xu X. *Int. J. Solids. Struct.*, 141:245–253 (2018)
8. Silling SA. *J. Mech. Phys. Solids*, 48(1):175–209 (2000)
9. Silling SA, Epton M, Weckner O, Xu J, Askari E. *J. Elasticity*, 88(2):151–184 (2007)
10. Tupek MR, Rimoli JJ, Radovitzky R. *J. Mech. Phys. Solids*, 263:20–26 (2013)